

# Utilization of low-cost activated carbon from rapid synthesis of microwave pyrolysis for WC nanoparticles preparation

Atikah Ali<sup>1\*</sup>, Rubia Idris<sup>2,3</sup>

<sup>1</sup>*Department of Chemistry, Faculty of Science, Universiti Teknologi Malaysia UTM, 81310 Johor Bahru, Johor, Malaysia*

<sup>2</sup>*Department of Thermodynamics and Fluid Mechanics, Faculty of Mechanical Engineering, Universiti Teknologi Malaysia UTM, 81310 Johor Bahru, Johor, Malaysia*

<sup>3</sup>*Faculty of Science & Natural Resources, University Malaysia Sabah UMS, Jalan UMS, 88400 Kota Kinabalu Sabah, Malaysia*

\*Corresponding author, Tel: (+60) 0111-2140463; E-mail: atikah.ali23@gmail.com, rubia.idris@gmail.com

Received: 30 June 2016, Revised: 30 August 2016 and Accepted: 10 October 2016

DOI: 10.5185/amlett.2017.6964

www.vbripress.com/aml

## Abstract

In this study, the low-cost activated carbon from pistachio shell waste was sought through experiments using rapid synthesis of microwave-induced pyrolysis. The effect parameters of activating agents and microwave power on the surface area and carbon yield were studied. The results revealed that, well-grown pore structures with the highest surface area ( $681.2 \text{ m}^2\text{g}^{-1}$ ) and the highest carbon yield (70.3%) were produced using  $\text{K}_2\text{CO}_3$  as an activating agent and 600 W power level exposed to a 15-minute irradiation. The activated carbon with the highest porosity (AC600) was subsequently utilized in the tungsten carbide (WC) preparation which employed a facile method of mechanical milling. Finally, a high-thermal treatment under inert conditions was performed to completely convert W into WC. The physicochemical properties of the catalyst were evaluated by  $\text{N}_2$  adsorption-desorption, XRD, FESEM and TEM. It was observed that, the tungsten carbide produced was small and uniform spherical nanoparticles with average diameters of 60 to 100 nm. High porosity and high surface area of catalyst support were identified as factors leading to a homogeneous distribution of metal catalyst. Therefore, the nanoparticles of WC produced were attributed to activated carbon with high porosity (AC600) due to well distribution of the tungsten crystal phase. Copyright © 2016 VBRI Press.

**Keywords:** WC, activated carbon, microwave, pyrolysis, nanoparticles.

## Introduction

Globally, one of the most predominantly and commercially vital edible nuts is the tree nut of pistachio; a genus of *Pistacia Vera L.* and the family of Anacardiaceae [1]. The cultivated pistachio of commerce is native in the Middle East majorly, United States and Mediterranean countries. According to the statistical analysis reported by the Food and Agriculture Organization (FAO), approximately 30 million metric tons of pistachio nut biomass waste is generated annually by the pistachio nut processing industries [2]. This agriculture waste is commonly disposed of by deposition in landfill or by open burning, whereas its conversion to value added products such as activated carbon would be preferable [3].

Over the years, carbon material has appeared to be efficient and remarkable in numerous application fields due to its easy operation, simple design, resistance towards contaminated substances and major capability in mitigating in a wide range of pollutants, even from the gaseous environment. The consequences of high demands

and price of commercial activated carbon have prompted researchers to endeavor in establishing the natural abundance and renewable resources with low cost as alternative feedstock for the fabrication of activated carbon. Accordingly, the literature pertaining more on the consumption of agricultural by-products (lignocellulosics) available from the fields or manufactured from the industrial manufacturing factory as source for renewable energy in vast amounts [4] is abundant. The feedstock from fresh plants or plant-derived materials serves as the most economical source because it is readily available in heap quantity, low-cost, appreciable hardness, and are renewable with high carbon content and low level of inorganic compounds [5, 25]. Besides, it has the potential in contributing toward economic growth and the ability to mitigate environmental impacts. The common raw materials used are wood, coconut shells, nut shells, palm kernel shells, and stone fruits.

Previously, the rudimentary methods for preparing activated carbon were divided into two categories, namely, physical activation and chemical activation [6]. The physical activation comprises primary carbonization

followed by regulating gasification under the action of oxidizing gases at high temperatures, while the chemical activation involves the precursor mixed with a chemical, carbonized and rinsed to synthesize AC products [7]. Numerous studies have been done on the synthesis of activated carbon via conventional heating furnace. However, all of these methods have noticeable drawbacks and limitations. Recently, microwave irradiation has attracted a widespread attention due to its capability of molecular level heating, which led to homogeneous and rapid thermal reactions [8-12]. Microwave induced has emerged as an innovative option to a greener environment and eco-friendly technology in synthesizing of activated carbon. Besides, the microwave applied in domestic and some industrial material processing in various technological and scientific areas pertaining to heat dielectric materials is widely discovered [13]. In addition to feedstock, preparation method also tremendously affects the properties, quality, and cost of activated carbon. The problems of the thermal gradient and the expensive cost of activated carbon preparation are possible to solve using a rapid microwave irradiation method. Many excellent results were achieved over the past few years, utilizing a microwave irradiation method for the preparation of activated carbon with a high surface area and a high carbon yield [14]. As compared to conventional heating, MW provides a unique method of transferring energy from source to the material. Basically, the microwave transfers the electromagnetic energy to thermal energy. The microwave energy is converted in the form of heat throughout their entire volume of materials and interacts directly into the particles by conductor, insulator and absorber interactions [8, 40]. The microwave irradiation usage causes a rapid activation process and heating rate, shorter processing times, minimal effects of differential synthesis and higher energy savings [15].

Activated carbon has been extensively used in various fields such as wastewater treatment, battery electrode, catalyst, gas separation and energy storage [2, 16-20]. In particular to high porosity, the mesoporous structure plays an important role for the applications involved in adsorbents of bulk molecules, catalyst support and gas storage. In the present approach, activated carbon is used as a catalyst support for the preparation of tungsten carbide catalyst. It is expected that the low-cost activated carbon with high porosity prepared via facile method of microwave-induced pyrolysis can act as a catalyst support to provide sufficient surface area for high dispersion of tungsten during the catalyst preparation. WC catalysts show an excellent catalytic activity in numerous catalytic reactions, such as, hydrodeoxygenation, hydrodesulphurization (HDS), hydrodenitrogenation and hydrodesulfurization [21-24]. The catalysts also show a great performance in liquid-phase reactions such as hydrogenation reaction, ethylene hydrogenation, ammonia oxidation, methanation and ammonium synthesis [25]. In fact, WC is also used as a catalyst for reactions, including alkane reforming, Fischer-Tropsch reaction transformation and synthesis of hydrocarbon isomerization materials [26, 27]. These carbide materials indicate a new class of highly active and selective

catalysts in application of petroleum, chemical and automotive industries.

Therefore, the objective of this study was to prepare low-cost activated carbon with relatively well-developed porosity from pistachio shell waste via microwave-induced pyrolysis. The study explored the feasibility of microwave system for synthesizing high porosity activated carbon. Several types of chemicals were used to investigate the effects of activating agent on the porosity, carbon yield and surface area of the activated carbon. The activated carbon with the highest porosity thus produced was subsequently utilized for the synthesizing of tungsten carbide. The characterizations of the end-products were determined by the Elemental analysis, N<sub>2</sub> adsorption-desorption, TGA, FESEM, XRD and FTIR.

## Experimental

### Materials

The pistachio shell waste was used as a feedstock in this experiment. It was washed with 0.1M HCl solutions to remove adhering dirt particles from the surface of the shells, before it was heated at 110 °C overnight to dry and to remove trapped moisture. A total of five chemical activating agents, namely, K<sub>2</sub>CO<sub>3</sub>, KOH, K<sub>2</sub>CO<sub>3</sub>, ZnCl<sub>2</sub> and H<sub>2</sub>SO<sub>4</sub> were used to enhance the porosity of the activated carbon. All the materials and chemicals were used as received without further purification.

### Preparation of activated carbon

Preparation of activated carbon from pistachio shell waste was performed using the five different activating agents and different microwave power levels at 450, 600, 700 and 800 W. The chemical impregnation ratio (2:1) and irradiation time (15 min) were fixed parameters in the optimizing of activated carbon preparation. An amount of dry pistachio shell with particle sizes of 5 – 10 mm was soaked into concentrated activating agent solution for 24 hrs. The slurry thus produced was transferred into a round-bottom flask with gas inlet and outlet tubes. To heat and activate the slurry, a microwave oven with suitable modification, operating at 2.45 GHz was used (Fig. 1). Nitrogen gas at a pre-set flow rate was used to purge air in the reactor before microwave irradiation started and it was let to continue to flow during the activation stage. At the end of the process, the product was left to quench at the ambient temperature under the same nitrogen flow rate. The activated carbon was washed repeatedly with hot distilled water until a pH value of 6 to 7 of the residual liquid was achieved. The sample was subsequently heated at 110°C overnight to dry before it was characterized further. The yield of the sample was calculated using the following equation:

$$\text{Yield (\%)} = \frac{\text{Weight of } AC_{PS}}{\text{Weight of } D_{PS}} \times 100\% \quad (1)$$

where,  $AC_{PS}$  is the activated carbon derived from pistachio shell waste and  $D_{PS}$  is the freshly dried pistachio shell waste. Samples prepared with the five different activating agents were denoted as AC1, AC2, AC3 and AC4, while samples prepared with the four different

microwave power levels were denoted as AC450, AC600, AC700 and AC800.

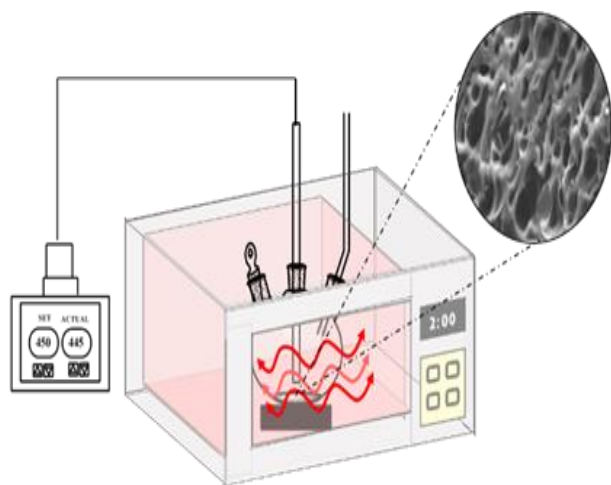


**Fig. 1.** Schematic diagram of rapid synthesis of activated carbon via microwave-induced pyrolysis [14,15].

#### Preparation of tungsten carbide (WC)

The facile method of mechanical milling was used in the tungsten carbide preparation. Approximately, 1.0 g of  $WO_3$  was mixed with 1.0 g of AC600 (1:1 ratio) before the mixture was milled at a rotation speed of 250 rpm for 48 hours. The mixture was later placed into a porcelain boat and loaded into the conventional heating furnace in a close-ended quartz tube equipped with inlet and out valves to allow for incoming and outgoing flow of the Nitrogen used for purging. The furnace was purged with the Nitrogen gas for 30 minutes before and after the experiment. The experiments were conducted at a temperature of  $950^\circ\text{C}$  with a heating rate of  $5^\circ\text{C min}^{-1}$  for 6 hours under a nitrogen atmosphere. The end product was denoted as WC-AC600 catalyst.

#### Characterization

The thermogravimetric analysis (TG-DTA) was performed on Mettler-Toledo TG50 to determine the moisture, ash, volatile matter and fixed carbon contents. The CHNS-O elemental analysis was conducted to evaluate the ultimate contents of carbon, hydrogen, nitrogen and sulphur. The surface functional group for chemical characterization of samples was detected using the potassium bromide (KBr) pellets with 1/100 ratio by Fourier Transform Infrared Spectrometer (FTIR) in the scanning range of  $400$  to  $4000\text{ cm}^{-1}$  for each sample. The surface area, pore size distribution, and pore volume of the sample were determined from the sorption isotherms using a non-local density functional theory (NLDFT) method using Beckman Coulter SA 3100 instrument [41,42]. The morphological properties of the product sample were performed using FESEM-EDX (ZEISS Supra 35 VP) and TEM (Philips EM420). The crystallinity of the catalysts were confirmed by X-ray diffraction (XRD) recorded on a Bruker Advance D8 X-ray powder diffractometer using  $\text{Cu K}\alpha$  radiation source ( $40\text{ kV}$ ,  $40\text{ mA}$ ) at a  $2\theta$  angle ranging from  $2$  to  $60^\circ$  with a scan rate of  $0.1^\circ$  continuously.

## Results and discussion

### Activated carbon

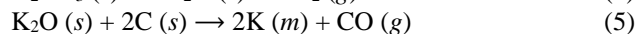
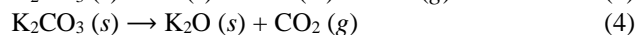
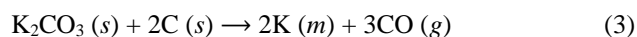
#### Effect of activating agent and microwave power level

Activating agent is one of the important variables in developing pore structure and carbon yield in synthesizing activated carbon [5, 28]. Fig. 2A shows the effect of different chemical activating agents on the surface area and carbon yield of activated carbon prepared at  $500\text{W}$  of microwave power. The figure revealed that, AC2 prepared using  $\text{K}_2\text{CO}_3$  had the highest carbon yield and surface area ( $69.5\%$ ,  $678.0\text{ m}^2\text{g}^{-1}$ ) followed by AC3, prepared using  $\text{ZnCl}_2$  ( $67.2\%$ ,  $653.1\text{ m}^2\text{g}^{-1}$ ) and AC1 prepared using  $\text{KOH}$  ( $64.9\%$ ,  $638.5\text{ m}^2\text{g}^{-1}$ ). The AC4 prepared using  $\text{H}_2\text{SO}_4$  was found to have the lowest carbon yield and surface area ( $52.7\%$ ,  $353.9\text{ m}^2\text{g}^{-1}$ ), due to the water vapor formed from the dehydration of  $\text{H}_2\text{SO}_4$  which increased the carbon burn off. The carbon yield also illustrated different results whereby, AC2 led in percentage, while AC4 had the lowest yield. The carbon yield gained by acid activating agent was low due to the strong oxidative nature of acids with their role as removers of carbon atoms [29]. In this study,  $\text{K}_2\text{CO}_3$  was found to be the best activating agent in term of carbon yield and surface area. The major distinct behavior could be explained by the different intercalation ability of K, Zn and H with the structural order and organization of the primitive material.

$\text{ZnCl}_2$  acted as a dehydrating agent during the activation that inhibited tar formation and any other liquids that could clog up the pores of the precursor [28]. Using  $\text{ZnCl}_2$  activation, the movement of the volatiles through the pore passages was not hindered and volatiles were released from the carbon surface with activation. During pyrolysis,  $\text{ZnCl}_2$  caused cellulose to degrade by dehydration, which caused aromatization of the carbon skeleton [30]. For potassium hydroxide (KOH) activation, it involved redox reduction and carbon oxidation to create porosity as shown in Eq. 2. The possible occurrence of active intermediates with carbon surface was the evolution of  $\text{CO}_2$ ,  $\text{CO}$  and  $\text{H}_2$  constituents throughout the activation process [5, 31].

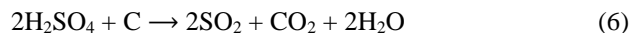


Concurrently, the reduction of  $\text{K}_2\text{CO}_3$  under inert conditions occurred to form potassium (K), potassium oxide ( $\text{K}_2\text{O}$ ),  $\text{CO}$  and  $\text{CO}_2$  as shown in Eq. 3 to 5 [32]. The generated carbonate and potassium metal would penetrate mildly into the internal structure of char surface, thus enlarging the existing pores and enhancing pore development in carbon structure and eventually increasing the surface area during activation step [33].



Conversely,  $\text{H}_2\text{SO}_4$  activation as an acid catalyst was considered the lowest among the five activating agents used, both in surface area and carbon yield. The

incorporation of sulphuric acid into the interior char matrix might inhibit the formation of tars (Eq. 6), thus promoting the introduction of oxygen functionalities of stable C-O complexes which accounted for the internal porosities [34].



Microwave power had an influential factor in affecting the surface area and carbon yield of activated carbon using  $\text{K}_2\text{CO}_3$  as an activating agent. **Fig. 2B** shows the surface area and yield percentage of all the activated carbon samples (AC450, AC600, AC700 and AC800). As presented in **Fig. 2B**, under a low microwave power of 450 W, the carbon yield and surface area achieved were, at 41.1 % and  $98.4 \text{ m}^2\text{g}^{-1}$ , respectively, which elucidated slow reactions between the char and the activation agent, causing incomplete growth on pore surface. In elevated microwave power level at 600 W, the activated carbon promoted expansion of carbon structure, thus increasing the carbon weight and surface area to 70.3% and  $681.2 \text{ m}^2\text{g}^{-1}$ , respectively, relative to released volatile material. However, it was found that, the surface area decreased from 493.2 to  $285.1 \text{ m}^2\text{g}^{-1}$  as the power level was further increased from 700 to 800 W, respectively. This was due to the decomposition of some volatile fractions which prompted a carbon burn over gasification [35]. This trend was similar with that found in previous studies on the preparation of activated carbon [36].

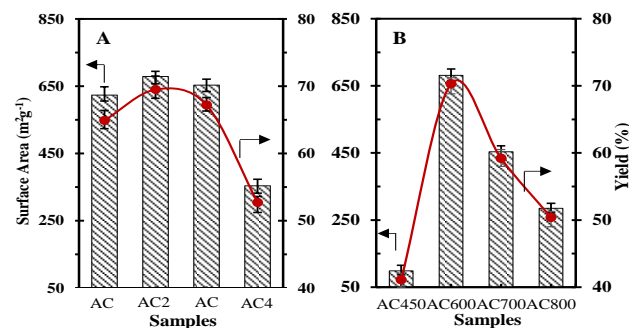


**Fig. 2.** Surface area and percentage yield of (A) AC1, AC2 AC3 and AC4; (B) AC450, AC600, AC700.

#### Characterization of activated carbon elemental analysis

Results of ultimate analysis of the chemical composition for C, O, H, N and S contents of raw pistachio shell, AC600 and activated carbon from previous studies were listed in **Table 1**. The carbon level of the pistachio shell waste, as indicated in the **Table 1**, increased after microwave reactions, although the oxygen, nitrogen and hydrogen contents showed the opposite trend. This was related to the degradation of organic substances and partial decomposition of volatile compounds under microwave irradiation, leaving a high purity carbon. The oxygen content steeply decreased from 49.77 % (raw PS) to 27.23% (AC600) due to the loss of oxygen-containing group (carboxylic and phenols) and oxygen-free Lewis sites (carbonyl group) at the edge of the carbon layers. The elemental analysis of the activated carbon in this study showed results which were well in agreement with

those in previous studies, despite different methods of preparation being used. The nitrogen content slightly decreased, whilst the sulphur content present in the raw pistachio shells and AC600 were thermally stable. The purity of contents of the pistachio shell element was found similar with that found in a previous research by Izquierdo et al. (2001), although they utilized a different type of pistachio shell waste [37].

**Table 1.** Properties of the raw pistachio shell and activated carbon.

Samples	Elements (wt.%)					Ref
	C	H	N	S	O <sup>a</sup>	
Raw PS	44.62	5.81	0.32	0.00	49.25	[34]
Raw PS	43.49	6.27	0.41	0.06	49.77	This study
AC	80.0	2.59	1.06	nm	17.1	[35]
AC600	76.13	2.54	0.15	0.08	27.23	This study

<sup>a</sup>. By different of 100% - ( $\Sigma\text{C}\% + \text{H}\% + \text{N}\% + \text{S}\%$ ); nm: Not mention

#### TGA and FTIR analysis

Thermogravimetric analysis (TGA) was used to study the pyrolytic characteristics and proximate contents of solid raw pistachio shell. The analysis and identification of decomposition stages by TGA and DTA of raw pistachio shell are shown in **Fig. 3A**. In the first stage (I), at the temperature range between 50 to  $100^\circ\text{C}$ , the derivative weight loss of 8.4% was recorded, attributable to the removal of water present (evaporation of moisture) in the material. In the second stage (II), a moderate weight loss of 7.5% occurred at the temperature range of 150 to  $300^\circ\text{C}$ . In the third stage (III), a significant weight loss of 58.9% occurred at the temperature range of 300 to  $400^\circ\text{C}$ , due to the removal of light volatile compounds.

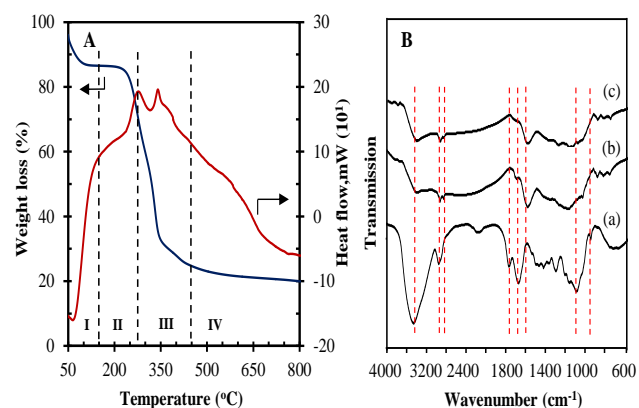


**Fig. 3.** (A) TG-DTA profile of raw PS; (B) FTIR spectra of (a) raw PS, (b) AC2 and (c) AC600.

After the major weight losses, the TG curve shows a long tail in the fourth (IV) stage at the temperature range of 400 to  $800^\circ\text{C}$  where the weight loss was 2.3 %. Stage IV was referred to as a passive pyrolysis stage because the final residue resembled a mixture of ash and fixed carbon [38]. At the temperature range of 200 to  $400^\circ\text{C}$ , the exothermic DTA peaks of raw PS were related to the decomposition of three major constituents, namely, hemicellulose, cellulose and lignin. As strongly agreed by Acikilin, (2012), hemicellulose, cellulose and lignin completed their decompositions at temperature intervals

of 210 to 325°C, 310 to 400°C and 160 to 900°C, respectively [37].

The FTIR spectra of raw pistachio shell, activated carbon prepared using  $K_2CO_3$  (AC2) and activated under 600 W microwave power level (AC600) are shown in Fig. 3B. The FTIR pattern presented in Fig. 3B was different from those of raw PS and activated carbon (AC2 and AC600). The intensity peaks of AC2 and AC600 decreased significantly after the samples were activated by microwave irradiation. A sharp band at approximately  $3430\text{ cm}^{-1}$  for raw PS (a) was assigned to O-H stretching vibration in hydroxyl groups of moisture content. A band was placed at around  $2900$  to  $2800\text{ cm}^{-1}$  in raw PS, AC2 and AC600 samples which contributed to C-H stretching vibrations in methyl and methylene groups. A band at  $2120\text{ cm}^{-1}$  was ascribed to (C=C) stretching vibrations in alkyne groups, while a band at  $1736\text{ cm}^{-1}$  was assigned to carbonyl (C=O) vibration, coming probably from aliphatic acids, esters or ketones.

For raw PS, a band at  $1380\text{ cm}^{-1}$  shell was ascribed to  $\nu(\text{C-O})$  stretching vibrations of medium intensity in carboxylate groups. A band at  $1200$  to  $1000\text{ cm}^{-1}$  for raw PS, AC2 and AC600 samples was known to belong to either ether, esters or phenol groups. In raw PS, the olefinic (C=C) in conjugated bond vibrations caused the band to appear at approximately  $1638\text{ cm}^{-1}$ . Small peaks at  $1118$  and  $1044\text{ cm}^{-1}$  were attributable to alcohol (R-OH) groups. In Fig. 3B for AC2 and AC600, the O-H vibration caused the hydroxyl group to disintegrate and to become a flat band in the range of  $3400$  to  $3300\text{ cm}^{-1}$ . The C-H vibration in methyl and methylene groups was hardly seen for AC2 and AC600, showing that there was a decline in aliphaticity caused by the heat treatment process. The skeletal C=C vibrations in aromatic rings of AC2 and AC600 was present in low band, where most of the band locations were in the range of  $1500$  to  $1100\text{ cm}^{-1}$ . The overall results obtained were in agreement with those found by Foo and Hameed, (2011) [33].

#### FESEM analysis

The effect of microwave power levels on the textural morphology of activated carbon was investigated using  $K_2CO_3$  at an impregnation ratio of 2:1 and irradiation time of 15 minutes, shown in Fig. 4. As depicted in Fig. 4A, under low microwave power levels of 450 W, the surface morphology of pore structure developed insufficiently, causing low continual reactions between char and activating agent. Soaring microwave power at 600W (Fig. 4B) resulted in the formation of clear micro-mesopore structures, due to the combined effects of internal and volumetric heating which caused enlargement of the carbon structure, thus producing a higher porosity and surface area [39].

However, at an elevated radiation power of 700 W (Fig. 4C), the absorbed microwave had more energy which contributed to an initial destruction of pore structures. At a higher power of 800 W (Fig. 4D), smaller micropores-mesopores began to expand and the larger pores collapsed which eventually led to the decrease in surface area. Based on the study by Foo and Hameed (2012), the rapid

reactions at higher thermal radiation would accelerate dehydration, devolatilization and decomposition [39].

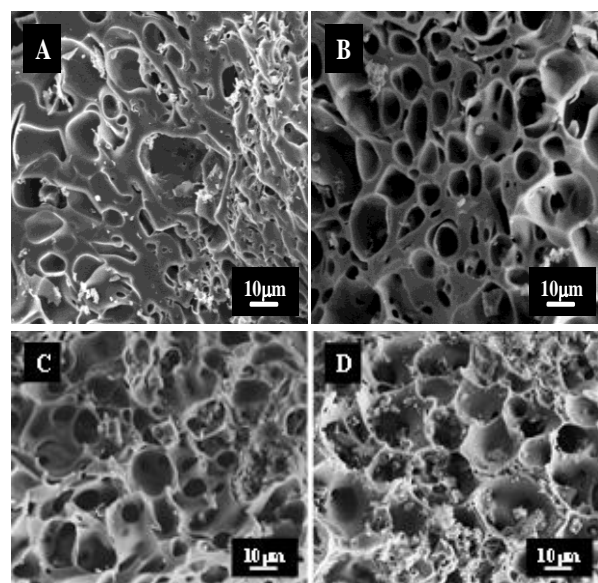


Fig. 4. FESEM images of (A) AC450 (B) AC600 (C) AC700 and (D) AC800 at a magnification of 1000x.

#### Characterization of tungsten carbide catalyst

##### $N_2$ adsorption-desorption analysis

The  $N_2$  adsorption-desorption isotherm of AC600 and WC-AC600 are shown in Fig. 5A. From the figure, it was obviously shown that, both isotherms samples were of type IV, indicating that the samples were mesoporous materials and the hysteresis loops type H4 indicated that the samples consisted of microspores structure. The two-step capillary condensation revealed that in the first step,  $P/P_0 = 0.4$ , attributable to mesopores structure inside the AC600 pores (intraparticle) [43]. At a higher partial pressure ( $P/P_0 = 0.9$ ), a small hysteresis loop was observed in AC600 and WC-AC600, due to interparticles textural porosity. This indirectly reflected the size of molecules, where a higher partial pressure was related to a smaller particle size. In contrast, the surface area and pore size of AC600 ( $681.2\text{ m}^2\text{g}^{-1}$ ) were found to decrease steeply upon W metal dissemination (WC-AC600,  $132\text{ m}^2\text{g}^{-1}$ ). This was due to the crystallite formation around the pore. Similar results were also observed by Moreno-Castilla et al. (2001), where the surface area and porosity of the carbon material decreased with increased W contents [44]. The results were well in agreement with FESEM images as shown in Fig. 4B and Fig. 6.

##### XRD Analysis

Fig. 5B shows the XRD patterns of the tungsten carbide catalyst, with three main peaks at  $2\theta = 31.51^\circ$ ,  $35.65^\circ$  and  $48.3^\circ$  observed in catalyst samples indexed as (001), (100) and (101) (JCPDS No. 00-051-0939), ascribed to the hexagonal type structure [45]. A small broad peak at  $2\theta \approx 20^\circ$  to  $30^\circ$  indicated that, the sample had amorphous structures attributable to the activated carbon (Fig. 5B insert). Sun et al. (2012) stated that the broad peak between  $2\theta \approx 20^\circ$  to  $30^\circ$  indicated that the average

particle size of WC on the catalyst support was within the range of nanoparticles size. Therefore, the dispersion of metal in nanoparticle sizes highly depended on the support's porosity [46]. Likewise, there was no impurity peaks of material, enhancement of carbon exploration by large mesoporous and formation of intermediate products were found which indicated that, the transformation of tungsten with activated carbon (AC600) was achieved and that, the sintering process reacted completely. Similar results were reported by Ma et al. (2007), who found that, as temperature increased to a higher level and reached 950 °C, the carburization of WO<sub>3</sub> occurred and it took almost six hours for the final products to gradually succeed in crystallinity transition from WO<sub>3</sub> to WC phase [45].

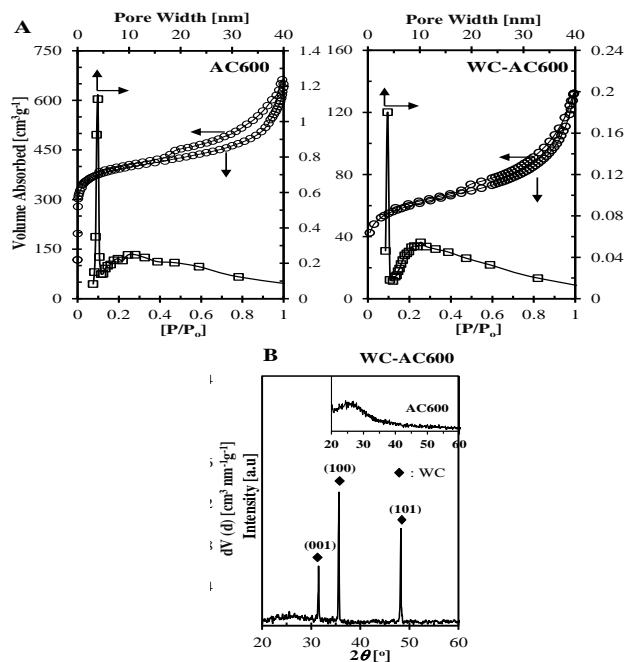


**Fig. 5.** (A) Nitrogen adsorption-desorption isotherms and NLDFT pore size distribution of AC600 and WC-AC600; (B) Wide angle of XRD pattern of WC-AC600 catalyst with AC600 (insert graph).

The average crystal diameter of the catalyst was estimated from the main peak marked from indices (100) plane using the Scherrer equation. The average crystal size of the catalyst was about 64.2 nm. Supports with high porosity and a high surface area, led to homogeneous distribution of WC metal. Therefore, the nanoparticles of WC produced was attributable to the high-porosity carbon, due to the well distribution of the tungsten crystal phase [47].

#### FESEM and TEM analysis

The FESEM images of WC-AC600, shown in **Fig. 6 A-B**, revealed the abundance of the catalyst with small and uniform spherical nanoparticles having average diameters of approximately 60 to 100 nm. The spherical nanoparticles were agglomerates with multifaceted grains attributable to the reduction and carburization during the WC preparation as shown in **Fig. 6B** [48]. It was also observed that, the outer surfaces of spherical nanoparticles comprised micro granules possibly

attributable to the activated carbon (**Fig. 6A**). For a more detailed morphological investigation, the sample was examined by using TEM (**Fig. 6 C-D**).

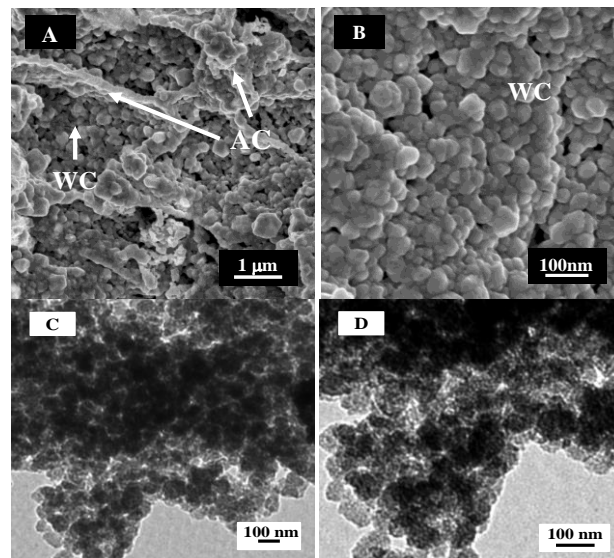


**Fig. 6.** (A-B) FESEM images and (C-D) TEM images of WC-AC600 catalyst.

From the images, it was clearly shown that, the tungsten carbide crystals were in agglomerated form due to the high surface area. The WC was observed to be in uniform spherical nanoparticles, demonstrating the success in synthesizing of WC nanoparticles catalyst using AC600.

#### Conclusion

Low-cost activated carbon from pistachio shell waste was successfully produced by rapid synthesis of microwave-induced pyrolysis. Well-grown pore structures with the highest surface area (681.2 m<sup>2</sup>·g<sup>-1</sup>) and the highest yield of activated carbon (70.3%) were produced at 600 W microwave power level using K<sub>2</sub>CO<sub>3</sub> as an activating agent. It was noteworthy that K<sub>2</sub>CO<sub>3</sub> was responsible for the diffusion of potassium element into the internal structure of char matrix, thus resulting in porous carbon with higher surface area. A suitable microwave power level at 600 W was found to be able to enhance the activation process. The activated carbon with the highest porosity (AC600) was utilized in the tungsten carbide preparation. From the N<sub>2</sub> adsorption-desorption study, it was revealed that, the surface area of AC600 (681.2m<sup>2</sup>·g<sup>-1</sup>) was found to decrease steeply upon W metal dissemination (132 m<sup>2</sup>·g<sup>-1</sup>), due to the crystallite formation around the pores. The results obtained were well in agreement with the FESEM images, which showed the catalyst being in abundance with small and uniform spherical nanoparticles having average diameters approximately between 60 to 100 nm. The spherical nanoparticles were agglomerates with multifaceted grains attributable to the reduction and carburization during the WC preparation. For detailed a morphological investigation, the sample was examined by using TEM. From the TEM images, it was clearly shown that, the tungsten carbide crystals were in agglomerated form due

to the high surface area. The uniform spherical nanoparticles of the WC observed demonstrated the success in synthesizing WC nanoparticles catalyst using AC600.

### Acknowledgements

The author gratefully acknowledges financial support received in the form of MyMaster scholarship (Atikah Binti Ali) from the Ministry of Higher Education, Malaysia (MOHE).

### References

- Polat, R.; Aydin, C.; Ak, B. E.; *Bulg. J. Agric. Sci.*, **2007**, *13*, 237.  
DOI: [www.agrojournal.org/13/02-12-07.pdf](http://www.agrojournal.org/13/02-12-07.pdf).
- SOPIB, Pistachios, Facts, Figures, Fertilizer Research. **2016**.
- Foo, K. Y.; Hameed, B. H.; *Bioresour. Technol.*, **2011**, *102*, 9814  
DOI: [10.1016/j.biortech.2011.07.102](https://doi.org/10.1016/j.biortech.2011.07.102)
- Nor, N.M.; Lau, L. C.; Lee, K. T.; Mohamed, A. R.; *J. Environ. Chem. Eng.*, **2013**, *1*, 658.  
DOI: [10.1016/j.jece.2013.09.017](https://doi.org/10.1016/j.jece.2013.09.017)
- Arie, A. A.; Vincent; Putranto, A.; *Adv. Mater. Lett.*, **2016**, *7*, 226.  
DOI: [10.5185/amlett.2016.6194](https://doi.org/10.5185/amlett.2016.6194)
- Arami-Niya, A.; Daud, W. M.; Mjalli, F. S.; *J. Anal. Appl. Pyrolysis*, **2010**, *89*, 197.  
DOI: [10.1016/j.jaap.2010.08.006](https://doi.org/10.1016/j.jaap.2010.08.006)
- Williams, P. T.; Reed, A. R.; *Biomass Bioenergy*, **2006**, *30*, 144.  
DOI: [10.1016/j.biombioe.2005.11.006](https://doi.org/10.1016/j.biombioe.2005.11.006)
- Mushtaq, F.; Mat, R.; Ani, F. N.; *Renewable Sustainable Energy Rev.*, **2014**, *39*, 555.  
DOI: [10.1016/j.rser.2014.07.073](https://doi.org/10.1016/j.rser.2014.07.073)
- Mushtaq, F.; Abdullah, T. A. T.; Mat, R.; Ani, F. N.; *Bioresour. Technol.*, **2015**, *190*, 442-450.  
DOI: [10.1016/j.biortech.2015.02.055](https://doi.org/10.1016/j.biortech.2015.02.055)
- Ania, C. O.; Parra, J. B.; Menendez, J. A.; Pis, J. J.; *Water Res.*, **2007**, *41*(15), 3299-3306.  
DOI: [10.1016/j.watres.2007.05.006](https://doi.org/10.1016/j.watres.2007.05.006)
- Liu, X.; Yu, G.; *Chemosphere*, **2006**, *63*(2), 228-235.  
DOI: [10.1016/j.chemosphere.2005.08.030](https://doi.org/10.1016/j.chemosphere.2005.08.030)
- Mubarak, N. M.; Sahu, J. N.; Abdullah, E. C.; Jayakumar, N. S.; *J. Anal. Appl. Pyrolysis*, **2016**, *120*, 521-528.  
DOI: [10.1016/j.jaap.2016.06.026](https://doi.org/10.1016/j.jaap.2016.06.026)
- Menéndez, J. A.; Arenillas, A.; Fidalgo, B.; Fernández, Y.; Zubizarreta, L.; Calvo, E. G.; Bermúdez, J. M.; *Fuel Process. Technol.*, **2010**, *91*(1), 1-8.  
DOI: [10.1016/j.watres.2007.05.006](https://doi.org/10.1016/j.watres.2007.05.006)
- Hesas, R. H.; Daud, W. M. A. W.; Sahu, J. N.; Arami-Niya, A.; *J. Anal. Appl. Pyrolysis*, **2013**, *100*, 1-11.  
DOI: [10.1016/j.jaap.2012.12.019](https://doi.org/10.1016/j.jaap.2012.12.019)
- Thostenson, E. T.; Chou, T. W.; *Composites, Part A.*, **1999**, *30*, 1055-71.  
DOI: [10.1016/S1359-835X\(99\)00020-2](https://doi.org/10.1016/S1359-835X(99)00020-2)
- Rahman, M. Z.; Ran, J.; Tang, Y.; Jaroniec, M.; Qiao, S. Z.; *J. Mater. Chem. A*, **2016**, *4*, 2445.  
DOI: [10.1039/C5TA10194H](https://doi.org/10.1039/C5TA10194H)
- Sethia, G.; Sayari, A.; *Carbon*, **2016**, *99*, 289-294.  
DOI: [10.1016/j.carbon.2015.12.032](https://doi.org/10.1016/j.carbon.2015.12.032)
- Kruse, N.; Schießer, Y.; Kämmnitz, S.; Richter, H.; Voigt, I.; Braun, G.; Repke, J. U.; *Sep. Purif. Technol.*, **2016**, *164*, 132-137.  
DOI: [10.1016/j.carbon.2015.12.032](https://doi.org/10.1016/j.carbon.2015.12.032)
- Barroso-Bogeat, A.; Alexandre-Franco, M.; Fernández-González, C.; Gómez-Serrano, V.; *Arabian J. Chem.*, **2016**.  
DOI: [10.1016/j.arabj.2016.02.018](https://doi.org/10.1016/j.arabj.2016.02.018)
- Zhu, W.; Ignaszak, A.; Song, C.; Baker, R.; Hui, R.; Zhang, J.; Campbell, S.; *Electrochimica Acta* **2012**, *61*, 198-206.  
DOI: [10.1016/j.electacta.2011.12.005](https://doi.org/10.1016/j.electacta.2011.12.005)
- Ranhotra, G. S.; Bell, A. T.; Reimer, J. A.; *J. Catal.*, **1987**, *108*(1), 40-49.  
DOI: [10.1016/0021-9517\(87\)90153-9](https://doi.org/10.1016/0021-9517(87)90153-9)
- Park, K. Y.; Seo, W. K.; Lee, J. S.; *Catal. Lett.*, **1991**, *11*(3-6), 349-356.  
DOI: [10.1007/BF00764327](https://doi.org/10.1007/BF00764327)
- Oyama, S. T. Introduction to the chemistry of transition metal carbides and nitrides, In The chemistry of transition metal carbides and nitrides; Oyama, S. T. (Eds.); Springer: Netherlands, **1996**, pp. 1-27.  
DOI: [10.1007/978-94-009-1565-7](https://doi.org/10.1007/978-94-009-1565-7)
- Ramanathan, S.; Oyama, S. T.; *J. Phys. Chem.*, **1995**, *99*(44), 16365-16372.  
DOI: [10.1021/j100044a025](https://doi.org/10.1021/j100044a025)
- Kirakosyan, K. G.; Manukyan, K. V.; Kharatyan, S. L.; Mnatsakanyan, R. A.; *Mater. Chem. Phys.*, **2008**, *110*(2), 454-456.  
DOI: [10.1016/j.matchemphys.2008.03.003](https://doi.org/10.1016/j.matchemphys.2008.03.003)
- Griboval-Constant, A.; Giraudon, J. M.; Twagishema, I.; Leclercq, G.; Rivas, M. E.; Alvarez, J.; Goldwasser, M. R.; *J. Mol. Catal. A: Chemical*, **2006**, *259*(1), 187-196.  
DOI: [10.1016/j.molcata.2006.06.015](https://doi.org/10.1016/j.molcata.2006.06.015)
- Patterson, P. M.; Das, T. K.; Davis, B. H.; *Appl. Catal., A*, **2003**, *251*(2), 449-455.  
DOI: [10.1016/S0926-860X\(03\)00371-5](https://doi.org/10.1016/S0926-860X(03)00371-5)
- Deng, H.; Yang, L.; Tao, G.; Dai, J.; *J. Hazard. Mater.*, **2009**, *166*(2), 1514-21.  
DOI: [10.1016/j.cej.2010.09.019](https://doi.org/10.1016/j.cej.2010.09.019)
- Foo, K. Y.; Hameed, B. H.; *Chem. Eng. J.*, **2012**, *184*, 57-65.  
DOI: [10.1016/j.cej.2011.12.084](https://doi.org/10.1016/j.cej.2011.12.084)
- Yorgun, S.; Vural, N.; Demiral, H.; *Microporous Mesoporous Mater.*, **2009**, *122*(1), 189-94.  
DOI: [10.1016/j.micromeso.2009.02.032](https://doi.org/10.1016/j.micromeso.2009.02.032)
- Ferrera-Lorenzo, N.; Fuente, E.; Suárez-Ruiz, I.; Ruiz, B.; *Fuel Process. Technol.* **2014**, *121*, 25-31.  
DOI: [10.1016/j.fuproc.2013.12.017](https://doi.org/10.1016/j.fuproc.2013.12.017)
- McKee, D. W.; *Fuel*, **1983**, *62*(2), 170-5.  
DOI: [10.1016/0016-2361\(83\)90192-8](https://doi.org/10.1016/0016-2361(83)90192-8)
- Foo, K. Y.; Hameed, B. H.; *Bioresour. Technol.*, **2011**, *102*(20), 9794-9.  
DOI: [10.1016/j.biortech.2011.08.007](https://doi.org/10.1016/j.biortech.2011.08.007)
- Izquierdo, M. T.; Rubio, B.; Mayoral, C.; Andrés, J. M.; *Appl. Catal., B*, **2001**, *33*(4), 315-24.  
DOI: [10.1016/S0926-3373\(01\)00192-8](https://doi.org/10.1016/S0926-3373(01)00192-8)
- Lua, A. C.; Yang, T.; *J. Colloid Interface Sci.*, **2004**, *274*(2), 594-601.  
DOI: [10.1016/j.jcis.2003.10.001](https://doi.org/10.1016/j.jcis.2003.10.001)
- Foo, K. Y.; Hameed, B. H.; *Bioresour. Technol.*, **2012**, *104*, 679-86.  
DOI: [10.1016/j.biortech.2011.10.005](https://doi.org/10.1016/j.biortech.2011.10.005)
- Açıklık, K.; *J. Therm. Anal. Calorim.*, **2012**, *109*(1), 227-35.  
DOI: [10.1007/s10973-011-1714-3](https://doi.org/10.1007/s10973-011-1714-3)
- Apaydin-Varol, E.; Pütün, E.; Pütün, A. E.; *Fuel*, **2007**, *86*(12), 1892-9.  
DOI: [10.1016/j.fuel.2006.11.041](https://doi.org/10.1016/j.fuel.2006.11.041)
- Foo, K. Y.; Hameed, B. H.; *Bioresour. Technol.* **2012**, *111*, 425-32.  
DOI: [10.1016/j.biortech.2012.01.141](https://doi.org/10.1016/j.biortech.2012.01.141)
- Fernández, Y.; Arenillas, A.; Menéndez, J. Á. Microwave Heating Applied to Pyrolysis, In Advances in Induction and Microwave Heating of Mineral and Organic Materials; Grundas, S. (Eds.); InTech: Austria, **2011**, pp. 723-52.  
DOI: [10.5772/13548](https://doi.org/10.5772/13548)
- Brunauer, S.; Emmett, P. H.; Teller, E.; *J. Am. Chem. Soc.*, **1938**, *60*(2), 309-319.  
DOI: [10.1021/ja01269a023](https://doi.org/10.1021/ja01269a023)
- Brunauer, S.; Deming, L. S.; Deming, W. E.; Teller, E.; *J. Am. Chem. Soc.*, **1940**, *62*(7), 1723-1732.  
DOI: [10.1021/ja01864a025](https://doi.org/10.1021/ja01864a025)  
DOI: [10.1063/1.1723871](https://doi.org/10.1063/1.1723871)
- Yuan, C.; Yao, N.; Wang, X.; Wang, J.; Lv, D.; Li, X.; *Chem. Eng. J.*, **2015**, *260*, 1-10.  
DOI: [10.1016/j.cej.2014.08.079](https://doi.org/10.1016/j.cej.2014.08.079)
- Moreno-Castilla, C.; Alvarez-Merino, M. A.; Carrasco-Marin, F.; Fierro, J. L. G.; *Langmuir*, **2001**, *17*(5), 1752-1756.  
DOI: [10.1016/j.cej.2014.08.079](https://doi.org/10.1016/j.cej.2014.08.079)
- Ma, J.; Zhu, S. G.; Ding, H.; Gu, W. S.; *Defect Diffus. Forum.* **2011**, *312-315*, 248-252.  
DOI: [10.1021/ja306913x](https://doi.org/10.1021/ja306913x)
- Sun, Z.; Sun, B.; Qiao, M.; Wei, J.; Yue, Q.; Wang, C.; Zhao, D.; *J. Am. Chem. Soc.*, **2012**, *134*(42), 17653-17660.  
DOI: [10.1021/ja306913x](https://doi.org/10.1021/ja306913x)
- Tallo, I.; Thomberg, T.; Kontturi, K.; Jänes, A.; Lust, E.; *Carbon*, **2011**, *49*(13), 4427-4433.  
DOI: [10.1016/j.carbon.2011.06.033](https://doi.org/10.1016/j.carbon.2011.06.033)

